Surfactant-Mediated Synthesis of a Novel Nanoporous Carbon−Silica Composite

Z.-M. Wang,*[,†,‡] K. Hoshinoo,[‡] K. Shishibori,[†] H. Kanoh,[§] and K. Ooi[‡]

PRESTO, Japan Science and Technology Corporation, Aquamaterial Separation Technology RG, Marine Resource and Environment Institute, National Institute of Advanced Industrial Science and Technology, 2217-14 Hayashi-cho, Takamatsu-shi, Kagawa 761-0395, Japan, and Center for Frontier Electronics and Photonics, Chiba University, 1-33 Yayoi-cho, Inage-ku, Chiba 263-8522, Japan

Received September 24, 2002. Revised Manuscript Received January 14, 2003

A novel nanoporous carbon−silica composite with medium hydrophilicity is synthesized by a series of methods consisting of preexpansion of the interlayer of graphite oxide (GO) by surfactant intercalation, the intercalation of tetraethoxylsilane (TEOS) and its hydrolysis in the interlayer, followed by post carbonization to form a robust bridged/pillared network. High-resolution N_2 adsorption results show that carbonization at 823 K gives a composite having the highest specific surface area of more than 1000 m^2/g with both microporosity and mesoporosity. Varieties of analytical results using DRIFT, NMR, XPS, and RAMAN spectra indicate that this composite contains small graphene sheets in its structure and its silicon components are silica particles with +4 valence. Morphology observation, thermal desorption, and other properties suggest the important roles of dispersion of GO in aqueous solution, preexpansion of GO interlayer, interlayer hydrolysis of TEOS molecules, and the carbonization condition in the formation mechanism of this nanoporous composite.

Introduction

Nanoporous materials having large internal surface areas and tailored pore shape/dimension have attracted great concern from the fields of adsorption/separation and heterogeneous catalysis.[1,2] One of the synthesis methods for obtaining a nanoporous material is the route from varieties of layered materials, including clay minerals and other two-dimensional framework materials, by soft chemical approaches such as chemical template,[3,4] intercalation,[5] and pillaring[6−8] processes. Graphite is a layered material having the thinnest atomic layer of all the layered materials.[9,10] A nanoporous material with thin graphitic layers has been expected from the aims of high efficiency adsorption and gas storage.[11,12] Highly expected materials for these purposes are the group of high-surface-area carbonaceous materials which are obtained by carbonization and activation of carbon precursors such as coal, pitch, natural nut shells, polymers, etc.[13] Despite a possible advantage of easy control to obtain a material having a large surface area and tailored pore geometries, preparation of nanoporous materials using graphite as the precursor has not yet been carried out by a soft chemical method. On the other hand, with respect to other nanoporous metal oxides such as zeolites, alumina, silica, etc., porous carbonaceous materials exhibit some peculiar merits in performance of specific adsorption and catalytic applications under moisture conditions, due to the coexistence of a hydrophobic surface and active centers constructed of surface functional groups.[14] Improvement of surface chemistry of the ordinary carbonaceous materials is generally carried out by surface modification in which the surface functional groups are selectively titrated and deposited by active species such as metal oxides/hydroxides, etc. However, there has not yet been any research to tailor a peculiar property onto a porous carbonaceous material by incorporating, or composing with, the aggregates of active species in the preparation/synthesis process.

Because of the neutral properties of the graphite walls, there is no driving force strong enough for a rigid species to expand and prop the graphitic layers to form an open pore system by the usual soft chemical methods.

* To whom correspondence should be addressed. Tel: (+)81-87-869-3574. Fax: (+)81-87-869-3550. E-mail: zm-wang@aist.go.jp.
† PRESTO, Japan Science and Technology Corporation.
‡ National Institute of Advanced Industrial Science and Technology.
§ Chiba University.

(1) Schubert, U.; Hüsing, N. *Synthesis of Inorganic Materials*; Wiley-VCH: Weinheim, Germany, 2000.
(2) Barton, T. J.; Bull, L. M.; Klemperer, W. G.; Loy, D. A.; McEnaney, B.; Misono, M.; Monson, P. A.; Pez, G.; Scherer, G. W.; Vartuli, J. C.; Yaghi, O. M. *Chem. Mater.* **1999**, 2633.
(3) Yanagisawa, T.; Shimizu, T.; Kuroda, K.; Kato, C. *Bull. Chem. Soc. Jpn.* **1990**, *63*, 988.
(4) Inagaki, S.; Fukushima, Y.; Kuroda, K. *J. Chem. Soc. Chem. Commun.* **1993**, 680.
(5) Barrer, R. M. *Zeolites and Clay Minerals as Sorbents and Molecular Sieves*; Academic Press: New York, 1978.
(6) Yamanaka, S.; Brindly, G. W. *Clays Clay Miner.* **1978**, *26*, 21.
(7) Pinnavaia, T. J. *Science* **1983**, *220*, 365.
(8) Landi, M. E.; Aufdembrink, B. A.; Chu, P.; Johnson, I. D.; Kirker, G. W.; Rubin, M. K. *J. Am. Chem. Soc.* **1991**, *113*, 3189.
(9) Marsh, H. *Introduction to Carbon Science*; Butterworth: London, 1989.
(10) Pierso, H. O. *Handbook of Carbons, Graphite, Diamond, and Fullerenes*; Noyes Publication: Park Ridge, IL, 1993.
(11) Dresselhaus, M. S.; William, K. A. *MRS Bull.* **1999**, *24*, 45.
(12) Matranga, K. R.; Myers, A. L.; Glandt, E. D. *Chem. Eng.* **1992**, *7*, 1569.
(13) Bond, R. L. *Porous Carbon Solids*; Academic Press: New York, 1967.
(14) Radovic, L. R.; Rodriguez-Reinoso, F. *Chem. Phys. Carbon* **1997**, *25*, 243.

10.1021/cm020965c CCC: $25.00
Published on Web 06/18/2003

Although the weak van der Waals-type bonding between the graphitic layers allows formation of the graphite intercalation compounds (GIC) for electrochemical/tribological application,[10,15] these materials are chemically instable in air and seem to have only small surface areas due to their "stuffing" sandwich structures. On the other hand, oxidation of graphite by strong oxidants gives a layered graphite oxide (GO), which shows excellent swelling and exfoliation properties similar to those of clay minerals.[16−25] The rich intercalation chemistry of GO makes it possible to accommodate in its interlayer space plenty of inorganic and organic species such as transitional metal ions,[26,27] polycations,[28] organic molecules,[23−25] and various kinds of polymers such as poly(ethylene oxide)s (PEO),[29] poly(furfuryl alcohol) (PFA),[30] and polyaniline (PA).[31] It may be thus possible to form a nanoporous material having thin carbon walls by adding a robust bridging/pillaring species into the interlayer of GO using a soft chemical method followed by an appropriate posttreatment such as carbonization. The synergy properties due to both the hydrophobic carbon surface and the specialties of the incorporated active species can then be expected from this kind of composite. Here, we report formation of this kind of nanoporous graphitic composite by preliminarily expanding the GO interlayer using a surfactant, followed by TEOS hydrolysis in the GO interlayer, and subsequent carbonization. The porosity and structural and surface properties of this composite will be characterized in detail, and a possible mechanism for formation of this composite will be proposed.

Experimental Section

Material Synthesis. A natural graphite (G) was oxidized in a mixture of concentrated sulfuric acid, fumed nitric acid, and potassium chlorate for 3 d using Staudenmaier's method[32] to obtain the graphite oxide (GO) with bright yellow color. A chemical formula of $C_8O_{3.7}H_{1.8}$ was obtained for this GO by carbon, oxygen, and hydrogen elemental analysis and after subtracting water content as determined from weight loss of GO in air up to 393 K. GO particles were then dispersed in a 0.05 N NaOH solution, upon which ultrasonic treatment was applied for 15 min, to obtain a stable and highly dispersed colloid solution. A 600 mL portion of $1.84 \times 10^{-3} - 11 \times 10^{-3}$ M hexadecyltrimethyl ammonium (C_{16}TMA) bromide aq. was then added dropwise into the GO colloidal solution, and the dispersed GO particles were aggregated by adsorbing surfactant and precipitated from the solution when stirring was stopped. The precipitates were filtered, completely washed with distilled water, and dried at 323 K in air overnight to obtain the surfactant-intercalated GO (GOC_{16}). About 398 mg of surfactant per g of GO was adsorbed to give GOC_{16} with a chemical composition of $C_8O_{3.7}H_{1.6}(C_{16}TMA)_{0.2}$. GOC_{16} was then treated in neat tetraethoxylsilane (TEOS) by 16 g/L of TEOS (or the TEOS/GOC_{16} molar ratio of 64:1) for one week. The product ($GOC_{16}S$) was centrifuged, washed with ethanol, and dried at 323 K overnight. The final products ($GOC_{16}S-T$) were obtained by evacuating $GOC_{16}S$ under various temperatures (room temperature to 823 K) or carbonizing it in a helium stream at 973 and 1173 K for 2 h.

Characterization. The microscopic features of G, GO, GOC_{16}, $GOC_{16}S$, and $GOC_{16}S-T$ were observed with a field-emission scanning electron microscope (FE-SEM, JEOL, JSM6330F type). The thermal gravimetry (TG) and differential thermal analysis (DTA) of GO, GOC_{16}, $GOC_{16}S$, and $GOC_{16}S-T$ were carried out under both a nitrogen and an air stream up to 1473 K with a Mac Science Co. Ltd. TG/DTA 2000 system. Temperature-programmed desorption (TPD) properties of GO, GOC_{16}, and $GOC_{16}S$ were measured in a helium stream with a constant flow rate of 50 STD mL/min at a ramp rate of 10 K/min using an Okurariken TP-5000 apparatus. Outgasses were analyzed by a Q-MASS spectrometer (ULVAC MMC-200).

The N_2 adsorption isotherms at 77 K on $GOC_{16}S-T$ were measured with a commercial volumetric apparatus (Belsorp 18A, Bellsorp Co.), which can measure the amount of adsorption from 1.32×10^{-4} kPa with an accuracy of 0.25% of the reading pressure values. The adsorption amount in the low-pressure range was calculated by the Takaishi−Sensui equation[33] after correction for pressure due to thermal transpiration effect. The $GOC_{16}S$-823 sample used for N_2 adsorption was supplied for a first-run water adsorption at 298 K after evacuation at room temperature (RT) for 2 h, and after the first-run water adsorption was again subjected to another (second-run) water adsorption after another preevacuation at RT for 2 h. For comparison, water adsorptions at 298 K on as-received commercial activated carbon fiber (ACF, Ad'all Co.) and hydroxyl silica were also measured after preevacuation at 393 K for 2 h.

The diffuse reflectance infrared Fourier transformation (DRIFT) spectrometry of G, GO, GOC_{16}, $GOC_{16}S$, and $GOC_{16}S-T$ were measured by a Nicolet NEXUS 470-type FT-IR spectrometer with a MCT ($Hg_{1-x}Cd_xTe$) detector. The equipment accessories and sample holder (whose temperatures were maintained at 333 K for G, GO, GOC_{16}, and $GOC_{16}S$, and at 393 K for $GOC_{16}S-T$) were purged by a continuous nitrogen flow (99.999% purity), and the DRIFT spectra were recorded from 256 scans in a resolution of 2 cm^{-1} after CO_2 species in air disappeared from the spectra.

^{13}C CP-MAS and ^{29}Si MAS NMR measurements were performed using a Bruker DSX-400 or a JEOL EX270 spectrometer operating at 100 or 67.9 MHz and 79.5 or 53.7 MHz, respectively. A MAS probe with zirconia rotors 7 or 6 mm in diameter was used. The spectra were obtained using 6 or 4.5 μS and 4.75 or 4.5 μS pulse widths together with 4 and 10 s delay time for ^{13}C and ^{29}Si, respectively. The spinning rate was 4900 or 6000 Hz for both the species and the contact time for ^{13}C cross relaxation experiments was 4 or 5 ms. More than 1024 and 14 000 scans, respectively, for ^{13}C and ^{29}Si were accumulated.

The C 1s and Si 2p spectra of the X-ray photoelectron spectroscopy (XPS) were measured under a vacuum of 10^{-6} Pa using Mg Kα radiation (10 kV/20 mA) with a Shimadzu ESCA-K1 apparatus. The XPS spectra were curve-fitted by a nonlinear least-squares iterative technique based on Gaussian

(15) Bailar, J. C., Jr.; Emeléus, H. J.; Nyholm, S. R.; Trotman-Dickenson, A. F. *Comprehensive Inorganic Chemistry*; Pergamon Press: Oxford, 1973.
(16) Hoffman, U.; Frenzel, A.; Csalan, E. *Liebigs Ann. Chem.* **1934**, *510*, 1.
(17) Scholz, W.; Boehm, H. P. *Anorg. Allg. Chem.* **1969**, *369*, 327.
(18) Nakajima, T.; Matsuo, Y. *Carbon* **1994**, *32*, 469.
(19) Hamwi, A.; Marchand, V. *J. Phys. Chem. Solids* **1996**, *57*, 867.
(20) Matsuo, Y.; Sugie, Y. *Carbon* **1997**, *35*, 301.
(21) Lerf, A.; He, H.; Forster, M.; Klinowski, J. *J. Phys. Chem.* **1998**, *102*, 4477.
(22) He, H.; Klinowski, J.; Forster, M.; Lerf, A. *Chem. Phys. Lett.* **1998**, *287*, 53.
(23) Dékány, I.; Krüger-Grasser, R.; Weiss, A. *Colloid Polym. Sci.* **1998**, *276*, 570.
(24) Matsuo, Y.; Hatase, K.; Sugie, Y. *Chem. Commun.* **1999**, 43.
(25) Liu, P.; Gong, K.; Xiao, P.; Xiao, M. *J. Mater. Chem.* **2000**, *10*, 933.
(26) Kovtyukhova, N. I.; Karpenko, G. A.; Chuiko, A. A. *Russ. J. Inorg. Chem.* **1992**, *37*, 566.
(27) Kotov, N. A.; Dékány, I.; Fendler, J. H. *Adv. Mater.* **1996**, *8*, 637.
(28) Kovtyukhova, N. I.; Ollivier, P. J.; Martin, B. R.; Mallouk, T. E.; Chizhik, S. A.; Buzaneva, E. V.; Gorchinskiy, A. D. *Chem. Mater.* **1999**, *11*, 771.
(29) Matsuo, Y.; Tahara, K.; Sugie, Y. *Carbon* **1997**, *35*, 113.
(30) Kyotani, T.; Moriyama, H.; Tomita, A. *Carbon* **1997**, *35*, 1185.
(31) Liu, P.; Gong, K. *Carbon* **1999**, *37*, 701.
(32) Staudenmaier, L. *Ber Dtsch. Chem. Ges.* **1989**, *31*, 1481.
(33) Takaishi, T.; Sensui, Y. *Trans. Faraday Soc.* **1963**, *59*, 2503.

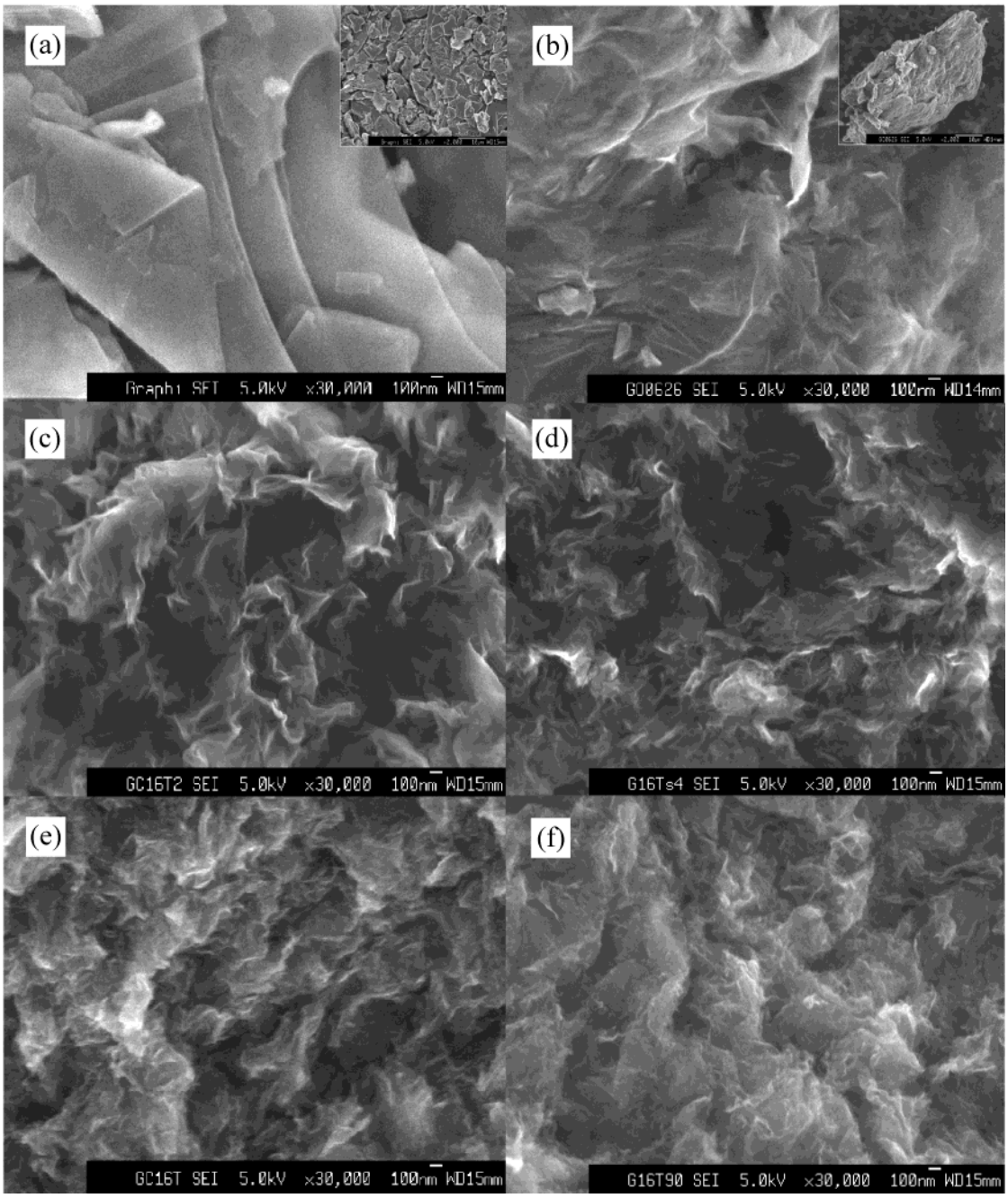

Figure 1. FE-SEM images (3×10^4 magnifications) of (a) G, (b) GO, (c) GOC_{16}, (d) $GOC_{16}S$, (e) $GOC_{16}S$-823, and (f) $GOC_{16}S$-1173. Insets in (a) and (b) are low magnification (2×10^3) images.

function after baseline subtraction using Shirley's method.[34] The position of the most intense carbon−carbon peak was taken as 284.6 ev. The full width at half-maximum values of the deconvoluted C 1s peaks were 2.2 ± 0.3 ev. The molecular contents of the oxygen-containing groups were calculated from the ratio of peak area of the corresponding deconvoluted peak to the total area.

RAMAN spectra of G, GO, and $GOC_{16}S$-823 in comparison with that of a commercial activated carbon (AC, Kansai Netsukagaku Co.) were collected with a Kaiser Optical Systems Inc. HoloProbe 532 system containing a continuous wave frequency-doubled Nd:YAG laser light with a wavelength of 532 nm and a CCD detector. Laser light with a power of 1 mW was focused onto the sample for 60 s and the spectra were collected by 2 scans at a resolution of 5 cm^{-1}.

(34) Brigg, D.; Seah, M. P. *Practical Surface Analysis*, 2nd ed.; John Wiley & Sons: New York, 1995.

Results and Discussion

Morphology and Thermal Desorption Properties. Figure 1 shows the FE-SEM images of G, GO, GOC_{16}, $GOC_{16}S$, $GOC_{16}S$-823, and $GOC_{16}S$-1173. Graphite is constructed of good crystalline particles, presenting clear platelike morphology with a particle size between 2 and 10 μm (as confirmed by low magnification photographs). Oxidation of graphite gives graphite oxide with large-size winkled layers; the hydrophilicity of GO due to plenty of oxygen-containing groups (OCG) makes them inclined to stack one over another by hydrogen bond through external OCG to form larger packed particles. Hydrophobic treatment of GO using surfactant leads to separating and disorderly aggregating of the layered particles; their curved planes randomly meet

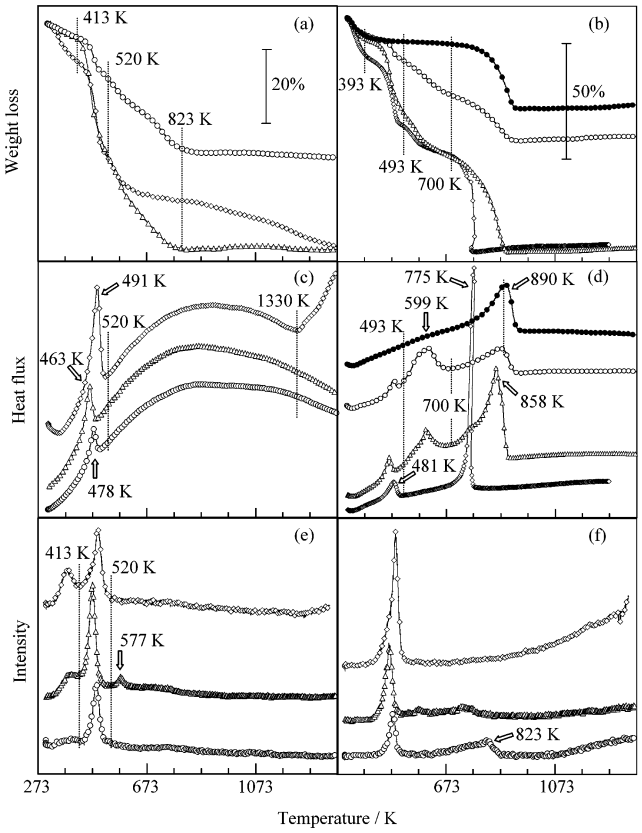

Figure 2. TG/DTA curves under N_2 ((a), (c)) and air ((b), (d)) streams, and TPD signals of m/e = (e) 18 (H_2O) and (f) 28 (CO) under He stream. Samples: ◇, GO; △, GOC_{16}; ○, $GOC_{16}S$; ●, $GOC_{16}S$-823.

with one another, presenting a structure of loosely packed assembly. This disordered structure is retained after TEOS treatment and even carbonization at 823 and 1173 K. It is well-known that GO has a pseudo-two-dimensional layered structure. A previous X-ray diffraction experiment has shown that the (001) repeating distance of GO (0.865 nm) can be expanded to 3.91 nm by C_{16}TMA ions intercalation, and no long-distance ordered structures can be found in the products treated with TEOS and carbonized at any temperature.[35] Nevertheless, the layer structure can still be clearly seen in these products from the FE-SEM images, indicating that, in these products, very thin carbon layered particles may randomly and completely mix, on a nanosize scale, with the silicon-related molecules/particles to form a composite. This result has also been confirmed by a previous high-resolution transmission electron microscopy (HRTEM) observation.[35] In the images of $GOC_{16}S$-823 and $GOC_{16}S$-1173, layer structures appear to be more closely packed by combination with the introduced silicon-related particles; the degree of packing increases with increased carbonization temperature. The layer size becomes smaller with respect to that in $GOC_{16}S$ probably due to the decomposition of the original GO layers in the process of carbonization.

Figure 2 a−d show the TG/DTA curves of GO, GOC_{16}, and $GOC_{16}S$ measured under both inert (nitrogen) and oxidizing (air) atmospheres. The TG/DTA curves in nitrogen atmosphere of all three samples contain three evident steps: (1) the dehydration step below 413 K, (2) the low-temperature GO layer decomposition step which gives a sharp DTA peak and a sudden weight loss at 463 to 491 K, and (3) the subsequent weight loss step after 520 K at which the GO decomposition peaks end, together with a broad DTA peak from 520 through 1330 K and a corresponding gradual evolution of H_2O and/or CO (Figure 2 e and f). Existence of step (3) indicates that one part of oxygen still deposits on the carbon surface after the major loss at the decomposition temperature (463−491 K). This step can thus be considered a low-temperature carbonization step in which active oxygen species evolve together with some hydrogen and carbon species under an inert condition. Furthermore, an exceptional step which gives rise to an upward DTA curve was observed for GO after 1330 K. A TPD result at the same condition shows the characteristic production of hydrogen (not shown for simplicity), indicating the start of poly-aromatization (graphitization) of carbon materials in the GO decomposed remains. It is interesting to notice that the low-temperature carbonization step of GO is different from those of the intercalated GO (GOC_{16} and $GOC_{16}S$). Whereas GO exhibits a gradual weight loss from 520 to 1373 K, low-temperature carbonization of GOC_{16} and $GOC_{16}S$ is almost complete in the range of 520 to 823 K, leaving an almost constant weight at temperature ranges between 823 and 1373 K. Elemental analysis shows the chemical composition of $GOC_{16}S$-973 to be $C_8H_{3.5}O_{7.7}Si_{3.5}$ or $C_8H_{3.5}O_{0.7}(SiO_2)_{3.5}$ by assuming formation of silica particles, indicating that only a small amount of oxygen remains on the carbon surface at 973 K for $GOC_{16}S$. This phenomenon implies that the OCGs on GO may interact with the intercalates (C_{16}TMA and TEOS) and become more easily detachable from the GO surface due to the enhanced reactivity.

Changes of OCG reactivity on GO by intercalation can also be confirmed from the lower temperature shift of the peaks responsible for the GO layer decomposition (491, 463, and 478 K for GO, GOC_{16}, and $GOC_{16}S$, respectively) and the TG/DTA activities under oxidizing atmosphere. In Figure 2 b and d, an additional peak at a medium temperature (around 599 K) can be observed for GOC_{16} and $GOC_{16}S$, but it is absent for GO which presents only two peaks responsible for GO layer decomposition at 481 K and burning of the carbon residuals at 775 K. The weaker carbon layer decomposition DTA peak for $GOC_{16}S$ becomes ambiguous, implying that one part of the OCG originally decomposed there interacts with TEOS molecules (Figure 2 d). Furthermore, the highest temperatures responsible for the carbon burning peaks for GOC_{16} and $GOC_{16}S$ (around 890 K) are much higher than that for GO (around 775 K) but very similar to that of 823-K-carbonized samples, indirectly manifesting the almost complete decomposition of OCG in GOC_{16} and $GOC_{16}S$ before their burning temperatures (Figure 2 d). Figure 2 e and f show the H_2O and CO_x evolution peaks for the three samples in TPD measurement under reductive atmosphere. In agreement with a smaller dehydration weight loss (Figure 2 a), the H_2O desorption peaks below 413 K become weaker by surfactant and TEOS intercalation due to the gradual hydrophobic change of GO.

(35) Wang, Z.-M.; Hoshinoo, K.; Xue, M.; Kanoh, H.; Ooi, K. *Chem. Commun.* **2002**, 1696.

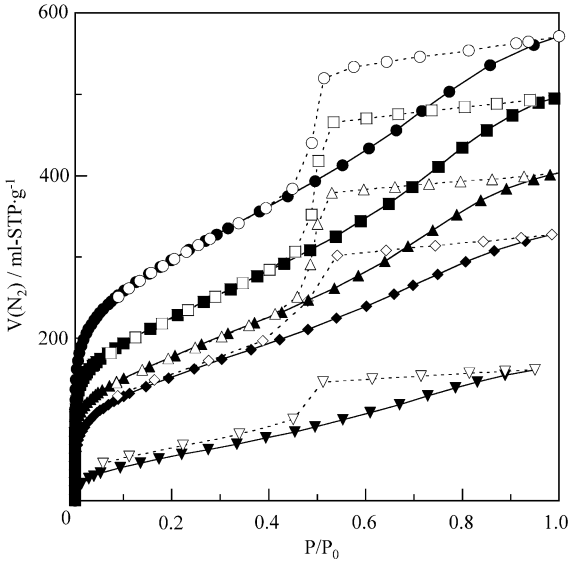

Figure 3. N_2 adsorption isotherms at 77 K on $GOC_{16}S-T$ with T = 393 (▼, ▽), 523 (◆, ◇), 823 (●, ○), 973 (■, □), and 1173 (▲, △) K. The solid and empty symbols represent the adsorption and desorption branches, respectively.

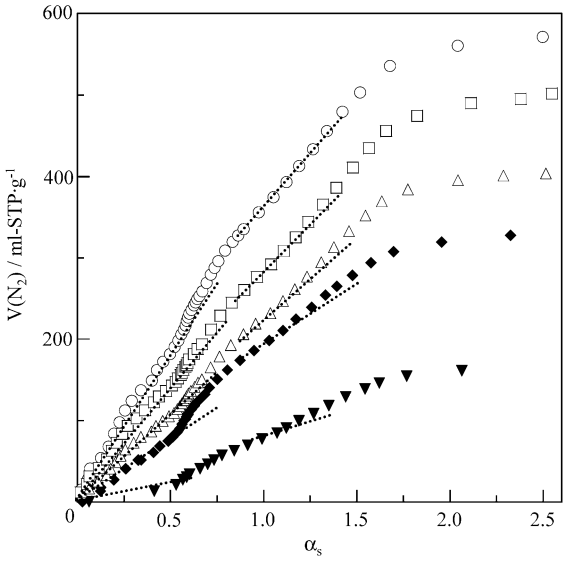

Figure 4. α_s Plots of N_2 adsorption isotherms on $GOC_{16}S-T$ with T = 393 (▼), 523 (◆), 823 (○), 973 (□), and 1173 (△) K.

The products of low-temperature GO layer decomposition are mainly H_2O and CO_x (CO or CO_2 or both). A small H_2O peak at 577 K together with some slight peaks due to NO_x species (not shown for simplicity) are observed for $GOC_{16,}$ which should come from decomposition of surfactant−OCG complex groups, thus confirming the above result. Furthermore, formation of new surface species after TEOS treatment can be confirmed from a broad peak characteristic of CO species at around 823 K for $GOC_{16}S$.

Porosity. Figure 3 shows the N_2 adsorption isotherms at 77 K on $GOC_{16}S$ after thermal decomposition under inert conditions (either by evacuation below 823 K or by thermal treatment in He stream above 973 K). The N_2 adsorption amount at first increases with increase of the evacuation temperature from the low-temperature GO layers decomposition at 523 K through the complete carbonization at 823 K, and in reverse decreases with the increase of carbonization temperature above 973 K. All these isotherms seem to consist of a steep uprising step at the initial P/P_0, a subsequent gradual increase step after $P/P_0 = 0.2$, followed by a greater increase step from $P/P_0 = 0.45$, together with an evident hysteresis desorption branch which closes at $P/P_0 = \sim 0.45$. Thus, the shape of adsorption isotherms may be considered to be a mixture of typical type I and type IV isotherms, which is derived from both the microporosity and mesoporosity in these samples.[36−38] The shape of each desorption branch is of typical H2 type,[38] indicating that the mesoporosities in these samples may be formed by aggregation of various plate particles, most possibly the carbon layers from GO or thermally decomposed residuals of GO with different sizes.

We applied the α_s-plot method to evaluate the pore structure and the pore evolution process. The α_s-comparison plot is a porosity-analyzing method that can simultaneously determine total, internal, and external surface areas, pore volume, and average pore sizes[37−40] and also an effective way to distinguish the microporosities from mesoporosities for a complex pore structure.[40] Figure 4 shows the α_s-plots from the nitrogen adsorption isotherms on $GOC_{16}S-T$, which were built up based on detailed standard adsorption data on a nonporous carbonaceous material.[39] Here, we adopt the nonporous carbonaceous material as the standard because the larger atomic parts of $GOC_{16}S-T$ are made of carbon as shown by the chemical analysis result (the materials appear as a black color). All the α_s-plots can be divided into three characteristic ranges corresponding to the shapes of their isotherms: (1) the range at $\alpha_s < 0.75$ which contains a linear part at the vicinity of $\alpha_s = 0.5$ ($P/P_0 = \sim 0.01$) whose extrapolation passes the origin; (2) the range at medium α_s values corresponding to the mesoporous uprising range, which contains a straight line range around $\alpha_s = 1.0$ ($P/P_0 = \sim 0.45$); and (3) the downward range above $\alpha_s = \sim 1.75$ ($P/P_0 = \sim 0.88$), where nitrogen molecules condense on the external surface. According to the two-step micropore filling mechanism[37] and subtracting pore effect (SPE) methods proposed by Kaneko et al.,[39] the upward swings below (USB) and above (USA) the straight line in the range (1) are the reflection of monolayer filling enhanced by the micropore field in ultramicropores (UMP) with a size of less than two molecular dimensions and the cooperative micropore filling involving the intermolecular interaction in supermicropores (SMP) with a size of 3 to 5 molecular dimensions, respectively. As there is no USB area appearing in the samples with $T < 523$ K, only larger micropores (SMP) as well as mesopores exist in these samples. Appearance of USB, USA, and the range (2) in α_s-plot of $GOC_{16}S$-823 indicates the coexist-

(36) Sing, K. S. W.; Everett, D. H.; Haul, R. A. W.; Moscou, L.; Pierotti, R. A.; Rouquerol, J.; Siemieniewska, T. *Pure Appl. Chem.* **1985**, *57*, 603.
(37) Gregg, S. J.; Sing, K. S. W. *Adsorption, Surface Area, and Porosity*; Academic: New York, 1982.
(38) Rouquerol, F.; Rouquerol, J.; Sing, K. S. W. *Adsorption by Powders & Porous Solids*; Academic: San Diego, CA, 1999.
(39) Kaneko, K.; Ishii, C.; Kanoh, H.; Hanzawa, Y.; Setoyama, N.; Suzuki, T. *Adv. Colloid Interface Sci.* **1998**, *76−77*, 295.
(40) Hanzawa, Y.; Kaneko, K.; Pekala, R. W.; Dresselhaus, M. S. *Langmuir* **1996**, *12*, 6167.

Table 1. Porous Parameters Calculated from α_s-Plot, BET, and DH Methods

sample	A_{BET} $m^2 \cdot g^{-1}$	$A_{s,total}$ $m^2 \cdot g^{-1}$	$A_{s,micro}$[a] $m^2 \cdot g^{-1}$	$A_{s,meso}$[a] $m^2 \cdot g^{-1}$	$A_{s,ext}$ $m^2 \cdot g^{-1}$	$V_{s,total}$ $m^2 \cdot g^{-1}$	$V_{s,micro}$[a] $m^2 \cdot g^{-1}$	$V_{s,meso}$[a] $m^2 \cdot g^{-1}$	$w_{s,micro}$ nm	$w_{s,meso}$ nm	w_{DH} nm
$GOC_{16}S$-393	220	210		150	60	0.18	-	0.18		2.4	2.0
$GOC_{16}S$-523	530	465	30 (6%)	375 (81%)	60	0.43	0.05 (12%)	0.38 (88%)		2.0	2.0
$GOC_{16}S$-623	670	590	105 (18%)	390 (66%)	95	0.47	0.08 (17%)	0.39 (83%)	1.5	2.0	2.0
$GOC_{16}S$-723	870	805	215 (27%)	540 (67%)	50	0.66	0.13 (20%)	0.53 (80%)	1.2	2.0	2.0
$GOC_{16}S$-823	1100	1035	335 (32%)	640 (62%)	65	0.83	0.18 (22%)	0.65 (78%)	1.1	2.0	2.0
$GOC_{16}S$-973	795	790	175 (22%)	560 (71%)	55	0.69	0.09 (13%)	0.60 (87%)	1.0	2.1	2.0
$GOC_{16}S$-1173	730	700	20 (3%)	640 (91%)	35	0.66	0.01 (2%)	0.65 (98%)	1.0	2.0	2.0

[a] Values in the parentheses are the ratio to $A_{s,total}$ or $V_{s,total}$.

ence of UMP, SMP, and mesopores in this sample. Micropores of $GOC_{16}S-T$ are seriously decreased by carbonization at $T > 973$ K as shown by the unapparent USB and USA ranges in their α_s-plots.

Because the total specific surface area, $A_{s,total}$, the sum of mesopore ($A_{s,meso}$) and external ($A_{s,ext}$) specific surface areas, the $A_{s,ext}$, the micropore volume, $V_{s,micro}$, and the sum of $V_{s,micro}$ and the mesopore volume ($V_{s,meso}$), can be calculated from the slopes of the straight lines in ranges (1), (2), and (3), and the interceptions of the straight lines in ranges (2) and (3), respectively,[40] each parameter for micropores and mesopores (including the micropore specific surface area, $A_{s,micro}$) can then be calculated. The average micropore ($w_{s,micro}$) and mesopore ($w_{s.meso}$) widths can be calculated by the following simple relationship:

$$w_{s,micro\ or\ meso} = 2(V_s/A_s)_{micro\ or\ meso} \quad (1)$$

Table 1 shows the calculated porous parameters and their ratios. For comparison, specific surface area, S_{BET} (calculated by the ordinary Brunauer−Emmett−Teller (BET) method) and the average mesopore size, w_{DH} (calculated by the Dollimore−Heal (DH) method) are also shown. The BET method generally has a tendency to overestimate the specific surface area for these samples with similarity to the results for porous carbonaceous materials.[39] The values of $A_{s,micro}$ or $V_{s,micro}$ gradually increase from 6% or 12% to 32% or 22%, respectively, at the highest case with the increase of evacuation temperature up to 823 K, and decrease again at the higher carbonization temperature, leaving an almost complete mesoporosity for $GOC_{16}S$-1173. Whereas the average size of micropore for each sample is between 1.5 and 1.0 nm, the average size of mesopore is small to 2 nm (a value in the boundary for definition of micropore and mesopore) in reasonable agreement with those from the DH method. Analysis of the pore-size evolution process reveals that the microporosity of $GOC_{16}S-T$ has a close relationship with the state of Si-related particles; it increases with the development of Si-related material-carbon plate composite network and decreases due to sintering of Si-related particles at a higher carbonization temperature.

DRIFT, NMR, and XPS Spectra. Figure 5 shows the DRIFT spectra of GO, GOC_{16}, $GOC_{16}S$, and $GOC_{16}S$-823. In correspondence to its hygroscopic property, a broad band at 3000 to 3500 cm^{-1} due to the H-bond water species can be observed in the spectrum of GO.

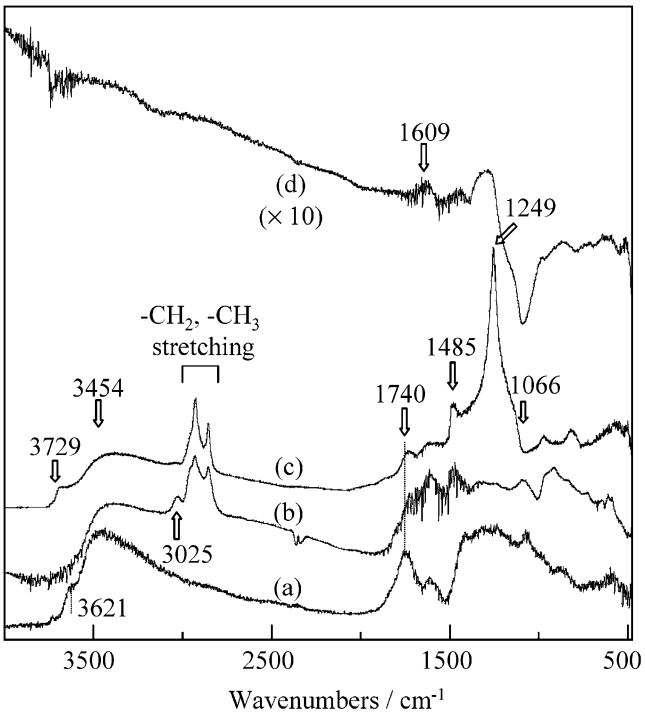

Figure 5. DRIFT spectra of (a) GO, (b) GOC_{16}, (c) $GOC_{16}S$, and (d) $GOC_{16}S$-823.

The intensity of this peak is weakened as a consequence of the hydrophobic change of the interlayer by surfactant and TEOS treatment, coinciding with the TG and TPD results. The peaks at 1740 and 3621 cm^{-1} (Figure 5 a) indicate the existence of C═O groups from carboxyl (−COOH) or carbonyl (−C═O) species and alcoholic −OH groups on GO, respectively.[41−43] Existence of nonreactive C═O species can be confirmed by a slight but evident peak at 1730 cm^{-1} which still remains after surfactant intercalation (Figure 5 b) and TEOS treatment (Figure 5 c). Complex overlapping of bands due to −COOH, −C−OH, and C−O species, and influence of H-bonding with water, result in a broad band between 1000 and 1415 cm^{-1} for GO (Figure 5 a). An evident peak at 1066 cm^{-1} is attributed to the epoxy species in the GO structure. Although there is not a characteristic IR band for tetraalkylammonium ions, their existence

(41) Fanning, P. E.; Vannice, M. A. *Carbon* **1993**, *31*, 721.
(42) Zawadzki, J. *Chem. Phys. Carbon* **1989**, *21*, 147.
(43) Matín Rodríguez, A.; Valerga Jiménez, P. S. *Carbon* **1986**, *24*, 163.

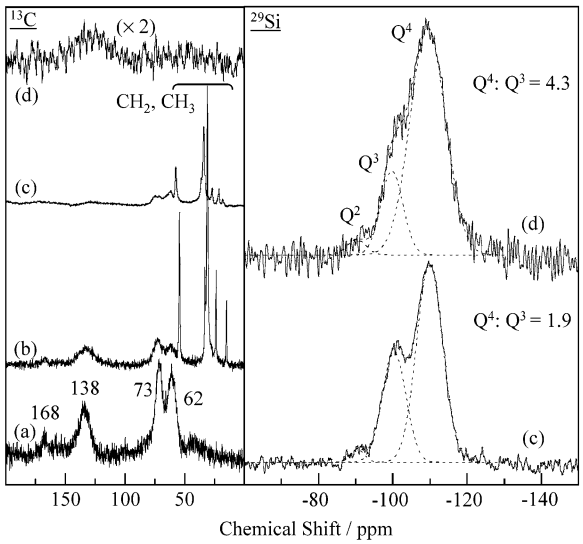

Figure 6. ^{13}C CP-MAS/NMR and ^{29}Si MAS/NMR spectra of (a) GO, (b) GOC_{16}, (c) $GOC_{16}S$, and (d) $GOC_{16}S$-823.

in GOC_{16} can be confirmed by the new peaks at 2850 to 3000 cm^{-1} due to the $-CH_2$ and $-CH_3$ stretching modes and a peak at 1485 cm^{-1} due to the $-CH_2$ or $-CH_3$ scissoring mode (Figure 5 b). Weakening or disappearing of −COOH and alcoholic −OH species by surfactant intercalation (Figure 5 b) indicates that surfactant molecules are mainly bonded on sites related to these species by ion-exchanging with H^+ ions. Hydrophobic treatment of GO by using surfactant makes it possible to observe a band at 3025 cm^{-1} (Figure 5 b), which can be assigned to the cyclic $-CH_2$ or epoxy-group-related −CH species existing in the vicinity of layer edges. TEOS treatment upon GOC_{16} gives rise to a very strong band at 1249 cm^{-1}, besides the aliphatic chain peaks at 2850 to 2965 cm^{-1} (Figure 5 c), whose position is blue-shifted from the ordinary position of the Si−O−Si bond (1000−1200 cm^{-1}).[44] Because existence of terminal silanol species can be seen clearly from the peak at 3729 cm^{-1} (Figure 5 c), we think that the species at 1249 cm^{-1} indicates the formation of highly cross-linked SiO_4 units in $GOC_{16}S$. After carbonization at 823 K, the peak due to SiO_4 units can also be detected, whereas those due to water and OCG on GO almost disappear (Figure 5 d). An evident peak at 1609 cm^{-1} (Figure 5 d) may possibly be ascribed to the C═C bond of polyaromatic rings[41] whose formation is accelerated by carbonization.

Figure 6 shows the ^{13}C CP-MAS/NMR and ^{29}Si MAS/NMR spectra of GO, GOC_{16}, $GOC_{16}S$, and $GOC_{16}S$-823. Klinowski et al. has recently carried out extensive research on the GO structure by using the NMR method.[21,22,45,46] According to their results, the ^{13}C peaks of GO at 62, 73, and 138 ppm can be ascribed to 1,2-epoxy C−O−C, alcoholic C−OH, and aromatic C═C species, respectively, in agreement with the structural proposal that aromatic rings are one part of the GO structure. The slight peak at 168 ppm is assigned to a small amount of carbonyl C═O species existing on GO. After intercalation or treatment of surfactant and TEOS, H^+ cross-polarized signals with strong intensities at 10−60 ppm are characteristic of aliphatic chains ($-CH_2$, $-CH_3$). The different positions of these peaks on GOC_{16} and $GOC_{16}S$ indicate substitution of one part of the surfactant by TEOS molecules. This result agrees with the chemical analysis results where nitrogen content decreases from 1.52 mmol/g in GOC_{16} to 0.69 mmol/g in $GOC_{16}S$.[35] After carbonization at 823 K, only a very weak peak at 138 ppm due to aromatic C═C bond remains, indicating not only the disappearance of OCG groups and almost all of the aliphatic chains due to TEOS and surfactant on GO, but also indirectly implying the in-plane growth of aromatic rings by releasing protons during carbonization. Moreover, we have measured ^{29}Si MAS/NMR spectra of $GOC_{16}S$ and $GOC_{16}S$-823 from −250 to 150 ppm. Signals at −90 to −130 ppm due to the cross-linked Si−O−Si bonds are observed, whereas no signal due to C−O−Si and C−Si (>−82 ppm) bonds has been found.[47,48] Signals from TEOS precursor (−82 ppm) were also not detected, indicating its little content. Peak splitting results show the main components to be Q^3 (one terminal −OH) at 100 ppm and Q^4 (without terminal −OH) species at 110 ppm with coexistence of small amounts of Q^2 (two terminal −OH) at 90 ppm for the two samples. Carbonization leads to detachment of large amounts of −OH groups and greatly increases polymerization of silica particles as shown by an increased Q^4 ratio.

To more quantitatively investigate the change of OCG on GO upon intercalation and carbonization, C 1s XPS spectra of GO, GOC_{16}, $GOC_{16}S$, and $GOC_{16}S$-823 were measured. Figure 7 a−d show the C 1s peaks which were deconvoluted into five components at 284.6, 286.4, 287.6, 288.6, and 290 ev due to C−C, C−OH/C−O (alcoholic −OH), C═O (carbonyl)/C−O−C (epoxy), O−C═O (carboxyl), and CO_3^{2-} species, respectively.[49] Table 2 shows the molar ratio of each species in each sample obtained by area comparison. A large part of the GO surface is covered by the OCG species (65%), manifesting its oxidized structure. The OCG contents in this GO precursor are mainly constructed of alcoholic −OH groups (about one-half) and carboxyl −COOH groups (35%) preferentially existing at the edges of GO layers; the content of −COOH seems to be much greater than the reported values of those prepared by other methods.[50] Shielding of OCG on GO by surfactant intercalates leads to a relative increase in C−C contents (not the substantial decrease in OCG groups). However, a relatively greater decrease in O−C═O ratio in comparison with C−OH ratio by surfactant intercalation indicates that the −COOH groups prefer to interact with the surfactant molecules. Furthermore, a greater decrease in the ratio of C−OH groups in comparison with that of −COOH groups in $GOC_{16}S$ implies that surfactant molecules preadsorbed on C−OH groups are more easily replaced by TEOS molecules. Whereas 18% of C−O groups still remain on the surface by carbonization of $GOC_{16}S$ at 823 K, almost all of the carbonyl/epoxy

(44) Dailey, J. S.; Pinnavaia, T. J. *Chem. Mater.* **1992**, *4*, 855.
(45) He, H.; Riedl, T.; Lerf, A.; Klinowski, J. *J. Phys. Chem.* **1996**, *100*, 19954.
(46) Lerf, A.; He, H.; Forster, M.; Riedl, T.; Forster, M.; Klinowski, J. *Solid State Ionics* **1997**, *101−103*, 857.
(47) Devreux, F.; Boilot, J. P.; Chaput, F.; Lecomte, A. *Phys. Rev. A* **1990**, *41*, 6901.
(48) Corriu, R. J. P.; Moreau, J. J. E.; Thepot, P.; Man, M. W. C. *Chem. Mater.* **1992**, *4*, 1217.
(49) Polovina, M.; Babić, B.; Kaluderović, B.; Dekanski, A. *Carbon* **1997**, *35*, 1047.
(50) Kovtyukhova, N.; Buzaneva, E.; Senkevich, A. *Carbon* **1998**, *36*, 549.

Table 2. Molar Ratios of Various Surface Species Obtained from C 1s XPS Deconvolution Result[a]

sample	C−C (284.6 ev)	C−OH, C−O (286.4 ± 0.1 ev)	C═O, C−O−C (287.6 ± 0.2 ev)	O−C═O (288.6 ± 0.1 ev)	CO_3^{2-} (290.0 ev)
GO	35%	31% (48%)	10% (17%)	23% (35%)	∼0
GOC_{16}	68%	23% (74%)	∼0	8% (26%)	∼0
$GOC_{16}S$	61%	18% (46%)	9% (23%)	12% (31%)	∼0
$GOC_{16}S$-823	73%	18% (67%)	3% (11%)	3% (11%)	3% (11%)

[a] Values in parentheses are the molar ratios of each group relative to the total OCG.

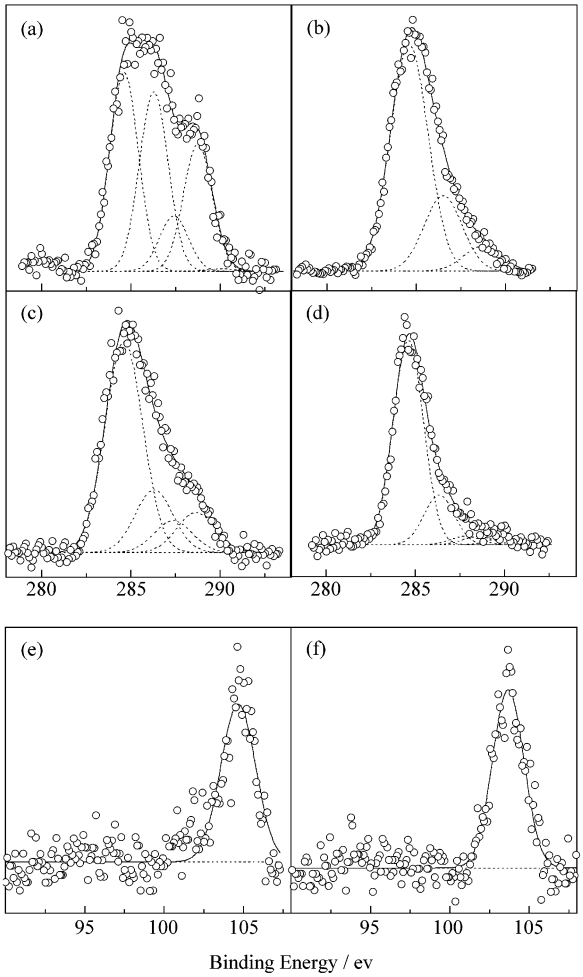

Figure 7. XPS spectra of (a) GO, C 1s; (b) GOC_{16}, C 1s; (c) $GOC_{16}S$, C 1s; (d) $GOC_{16}S$-823, C 1s; (e) $GOC_{16}S$, Si 2p; and (f) $GOC_{16}S$-823, Si 2p.

and carboxyl groups disappear, making the total OCG amount of $GOC_{16}S$-823 as low as about one-quarter. Figure 7 e and f also shows the Si 2p XPS spectra of $GOC_{16}S$ and $GOC_{16}S$-823. Each spectrum shows only a symmetric peak at ∼103 ev due to the Si^{4+} species; no evident peak or satisfactory deconvolution peak due to the suboxides such as Si^{3+}, Si^{2+}, etc. (100∼102 ev), or silicon (99.1 ev), or C−Si^{4+}−O (101 ev) and C−O−Si (102.7 ev) [51,52] can be detected. This result indicates that the silicon species in $GOC_{16}S$-823 are the silica particles with +4 valence state even though it was produced at a reductive carbonization condition. This result well coincides with those from the NMR results.

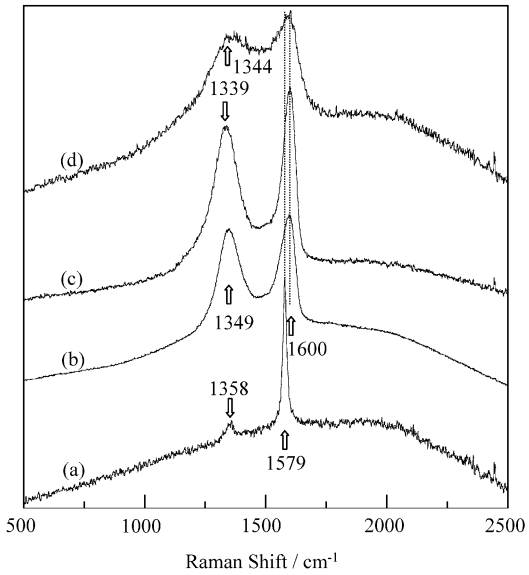

Figure 8. RAMAN spectra of (a) G, (b) GO, (c) $GOC_{16}S$-823, and (d) AC.

Comparative RAMAN Spectra and H_2O Adsorptivity. Figure 8 shows the RAMAN spectra of G, GO, and $GOC_{16}S$-823 in comparison with that of an ordinary microporous activated carbon (AC). G presents a sharp peak at 1580 cm^{-1} with a very slight nonsymmetric tailing toward the higher wavenumber side and a very weak peak at 1358 cm^{-1}. These peaks are assigned to the doubly degenerate deformation vibration of the E_{2g} mode of graphitic hexagonal rings (G band) and slight amounts of disordered (defect) structures in the graphite crystalline (D′ and D bands at 1620 and 1358 cm^{-1}, respectively).[53,54] Oxidation of G gives GO, which presents two broad bands at 1349 (D band) and 1600 cm^{-1} (the mixture of G and D′ bands) with an almost equal intensity, in agreement with the fact that some aromatic ring structures exist in GO as confirmed by the above NMR result. Surfactant and TEOS treatment do not greatly change the position and the shape of RAMAN spectra (not shown for simplicity). However, carbonization of $GOC_{16}S$ at 823 K leads to the peak at 1600 cm^{-1} becoming narrower with a higher relative intensity; the D band shifts to 1339 cm^{-1}, being a position close to that of AC. We also examined the RAMAN spectra of other porous carbonaceous materials such as ACF, nutshell char, and ACs with different degrees of activa-

(51) NIST X-ray photoelectron spectroscopy DATABASE20 2000, Ver. 3.5 (Web Version).
(52) Avila, A.; Montero, I.; Galán, L.; Ripalda, J. M.; Levy, R. *J. Appl. Phys.* **2001**, *89*, 212.
(53) Nakamizo, M.; Kammereck, R.; Walker, P. L., Jr. *Carbon* **1974**, *12*, 259.
(54) Turnstra, F.; Koenig, J. L. *J. Chem. Phys.* **1970**, *53*, 1126.

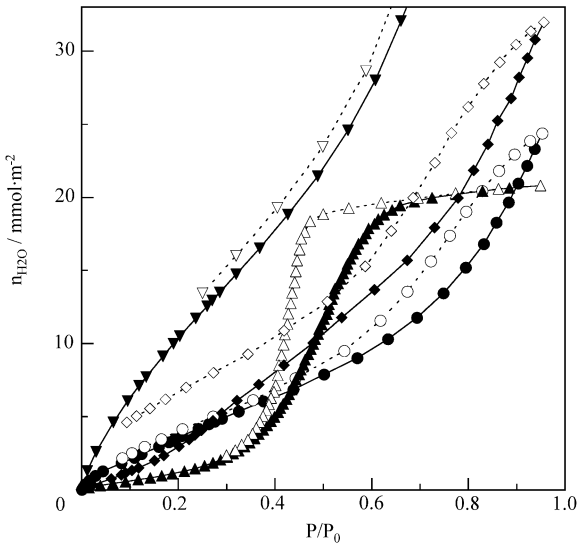

Figure 9. Comparison of water adsorption isotherms at 298 K on (a) $GOC_{16}S$-823 first run (◆, ◇), (b) $GOC_{16}S$-823 second run (●, ○), (c) AC (▲, △), and (d) hydroxyl silica (▼, ▽). The solid and empty symbols represent the adsorption and desorption isotherms, respectively.

tion. All these measurements show the same D band at ~1340 cm^{-1} and another band at 1600 cm^{-1} for these samples. Therefore, the carbon component in $GOC_{16}S$-823 somehow has a micrographitic structure similar to that existing in the ordinary porous carbonaceous materials.[39] Matsuo et al. have reported that even low-temperature pyrolytic treatment of GO gives a carbon product with graphene sheets and a higher repeating (002) distance (~0.4 nm).[20] Because of the layered structure of the GO precursor, we believe that the graphene sheets are more easily formed by carbonization of $GOC_{16}S$ with respect to the ordinary ACs or ACFs. Actually, a large amount of small graphene sheets of 1−3-nm size can be found easily from the HRTEM image previously reported.[35]

Figure 9 shows the first- and second-run H_2O adsorption isotherms on $GOC_{16}S$-823 in comparison with those on ACF and hydroxyl silica. In correspondence to the hydrophobic property, the H_2O adsorption isotherm on ACF shows a typical type V, presenting a small H_2O adsorption at small P/P_0 and a sudden uprising at the medium P/P_0 with a closed hysteresis branch. In contrast, there is a great increase in H_2O adsorption at small P/P_0 on silica, indicating the higher interaction energy between H_2O and the silica surface. On the other hand, the degree of uprising at small P/P_0 in H_2O adsorption isotherms on GOC_{16}-823 is between those on ACF and hydroxyl silica, manifesting that the hydrophilicity of this composite is between those of ACF and silica. The hydrophilicity of GOC_{16}-823 mainly comes from the bridged silica particles having the silanol groups, which strongly interact with the introduced H_2O molecules to form an irreversibly adsorbed water monolayer. The desorption loop of first-run H_2O adsorption is not closed whereas that of the second run is closed because of saturation of the −OH species in the first-run adsorption.

Formation Mechanism of Nanoporous Carbon−Silica Composite. Figure 10 schematically describes the formation mechanism of nanoporous $GOC_{16}S$−T. GO is known as a pseudo-two-dimensional material, which contains −COH groups in the interlayer space and −COOH groups in the layer edges. Despite varieties in the dissociative abilities of −COH groups in water, exertion of an appropriate alkaline condition makes most of the protons dissociate from the −COH and −COOH groups on GO, leaving a naked carbon layer skeleton with negative charges. Thus, a stable colloidal solution can be formed by the inter-repulsion of the electric-double-layered particles of the single carbon layers (Figure 10 b). As the delaminated carbon layers are highly exposed, they can easily interact and adsorb the positively charged surfactant ions to form heavy aggregates and precipitate from the solution upon introduction of surfactant (Figure 10 c). Although one part of the surfactant molecules adsorbed on hardly dissociative C−OH groups can be washed out by water from this aggregate, most of those adsorbed on −COOH groups and those forming orderly arranged aggregates in the carbon interlayer are retained by either the strong electrostatic interaction or an enhanced intermolecular hydrophobic interaction. TEOS molecules can then be hydrolyzed by interaction with the water contained in the interlayer of the aggregate (c). The disordered structure of $GOC_{16}S$ can be attributed to the formation of polymerized silica particles with different sizes due to the heterogeneous hydrolysis of TEOS molecules (Figure 10 d). TEOS may also possibly interact with the C−OH or $C-O^-(C_{16}TMA^+)$ species in GOC_{16} although clear evidence for the bonding species cannot be obtained in this research. Another possibility is that the OCG groups on GO react with intercalates upon exertion of elevated temperature, which accelerates their detachment from the carbon surface. Carbonization of $GOC_{16}S$ leads to fragmentation of the GO carbon layers, highly dispersed silica particles, and the desorption of organic impurities, thus forming a nanoporous network structure of the decomposed carbon layers bridged by silica particle aggregates. Therefore, dispersion of GO, interlayer hydrolysis of TEOS, and carbonization condition play important roles in formation of this kind of carbon−silica composite.

Conclusion

A novel nanoporous carbon−silicon composite is synthesized by preliminarily expanding the interlayer of graphite oxide using surfactant, followed by tetraethoxylsilane (TEOS) hydrolysis in the interlayers to form a silicon-related material-bridged/pillared network, and subsequent carbonization. Morphology observation demonstrates that the delaminated carbon layer structure from dispersion in sodium hydroxide aq. remains after surfactant intercalation, TEOS hydrolysis, and carbonization. Desorption of OCG on GO is accelerated by interaction with the surfactant-intercalated and TEOS molecules. N_2 adsorption results show that the porosity of this composite has a close relationship with the carbonization temperature: carbonization at 823 K gives rise to the highest specific surface area of more than 1000 m^2/g and a porous system with both micropores and mesopores having average sizes of 1.1 and 2.0 nm, respectively. DRIFT, NMR, XPS, and RAMAN results indicate that this composite contains small graphene sheets, exhibiting a macroscopic property due

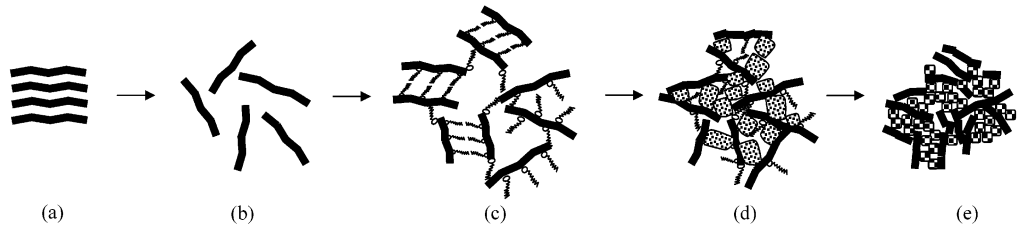

Figure 10. Schematic description of formation mechanism for nanoporous carbon−silica composites: (a) GO, (b) dispersed GO layers in alkali solution, (c) GOC_{16}, (d) $GOC_{16}S$, and (e) $GOC_{16}S$-823.

to the disordered micrographitic structure; its silicon components are silica particles with +4 valence. The intermediate water adsorptivity of this composite implies that its hydrophilicity due to the silica components it contains is between those of the ordinary porous carbonaceous material and the hydroxyl silica. Discussion of the formation mechanism suggests the important roles of GO dispersion in aqueous solution, interlayer preexpansion, subsequent hydrolysis of TEOS molecules, and carbonization condition in obtaining this kind of nanoporous composite.

Acknowledgment. Dr. M. Yamaguchi is gratefully acknowledged for his help in measurement of one part of the NMR spectra.

CM020965C